Journal of Alloys and Compounds 498 (2010) 157–161

Contents lists available at ScienceDirect

Journal of Alloys and Compounds

journal homepage: www.elsevier.com/locate/jallcom

Structural and magnetic properties of $BaFe_{12-2x}Ti_xRu_xO_{19}$

I. Bsoul[a,*], S.H. Mahmood[b,1], Abdel-Fatah Lehlooh[b,2]

[a] Physics Department, Al al-Bayt University, Mafraq 130040, Jordan
[b] Physics Department, Yarmouk University, Irbid 211-63, Jordan

ARTICLE INFO

Article history:
Received 7 February 2010
Received in revised form 14 March 2010
Accepted 16 March 2010
Available online 23 March 2010

Keywords:
Ball milling
Barium hexaferrite
Coercive field
Magnetization
Hyperfine parameters
Hopkinson peak

ABSTRACT

Barium hexaferrite samples $BaFe_{12-2x}Ti_xRu_xO_{19}$ were prepared by ball milling and their structural and magnetic properties were investigated using X-ray diffraction, TEM, Mössbauer spectroscopy, and vibrating sample magnetometry. It was found that the particle size increases appreciably, and the crystallinity improves with Ti–Ru substitution. Mössbauer spectroscopy revealed that the substitution of Fe^{3+} ions occurs at the $4f_2$ and $4f_1 + 2a$ sites for low substitution, and substitution at the $2b$ site occurs for $x \geq 0.2$. The saturation magnetization increases up to $x = 0.2$, and then starts to decrease for higher x values, while the coercivity decreases monotonically, recording a reduction of 55% at $x = 0.4$. These results were interpreted in terms of the site preferential occupation of the Ti^{2+} and Ru^{4+} ions. The thermomagnetic curves for all samples showed Hopkinson peaks indicating the presence of small superparamagnetic particles in the samples. The sample with $x = 0.0$ was found to consist of purely superparamagnetic particles, while the substituted samples were found to contain only 22–30% of the powders' mass as superparamagnetic particles.

1. Introduction

Barium hexaferrite $BaFe_{12}O_{19}$ (BaM) has been a subject of increasing interest since its discovery several decades ago. The magnetic properties of hexaferrites, such as their high saturation magnetization, corrosion resistivity, large magnetocrystalline anisotropy and high coercive field [1–5], and their low cost of production have generated considerable attention to these materials. In order to satisfy the utilization requirements of this compound in recording media, permanent magnets, microwave devices and magneto-optics, etc. [6–8], many studies have focused on tailoring hexaferrites with modified magnetic properties by substituting Fe^{3+} ions with divalent, trivalent and tetravalent cations or cations combinations [9–18]. For this purpose, several methods have been used to prepare hexaferrite particles including sol–gel method [19,20], mechano-combusition method [21], microwave-induced hydrothermal reaction [22], ammonium nitrate melt technique [23], reverse micelle technique [24], citrate–nitrate gel combustion method [25], co-precipitation method [26] and ball milling method [27,28]. Ball milling method is a technique that has been recently adopted for the preparation of barium ferrite powders, due to its simplicity in operation and handy experimental equipment [29]. Also this method is useful for the production of powders consisting of fine particles smaller than the single-domain size. The preparation method and the type of cation doping were found to have significant influence on the magnetic properties of barium hexaferrite.

The intrinsic magnetic properties of BaM are strongly dependent on its hexagonal structure. The structural stacking of $BaFe_{12}O_{19}$ layers is of the type RSR*S*, where R* and S* are obtained from the blocks R and S, by rotation of 180° around the hexagonal c-axis. The ferric ions are distributed among five crystallographic sites. There are three octahedral sites ($12k$, $4f_2$ and $2a$), one tetrahedral site ($4f_1$) and one trigonal bipyramid site ($2b$) [30–32]. The spin-up Fe^{3+} ions are distributed with one ion at the $2a$, one at the $2b$, and six at the $12k$ sites, while the spin-down Fe^{3+} ions are distributed with two at the $4f_1$ and two at the $4f_2$ sites. Accordingly, the magnetic moment per formula can be expressed as follows:

$$m = \vec{2a} + \vec{2b} + \vec{12k} + \overleftarrow{4f_1} + \overleftarrow{4f_2} \quad (1)$$

The anisotropy field H_a for uniaxial barium hexaferrite particles can be expressed as:

$$H_a = \frac{2K_1}{M_s} \quad (2)$$

where K_1 is the magnetocrystalline anisotropy constant, and M_s is the saturation magnetization. Based on the single ion model, Xu et al. [33] calculated the magnetocrystalline anisotropy constant for an Fe^{3+} ion at each of the five sites, and found that Fe ions provide

* Corresponding author. Tel.: +962 2 6297000x2127; fax: +962 2 6297031.
E-mail addresses: Ibrahimbsoul@yahoo.com (I. Bsoul), mahmoods@yu.edu.jo (S.H. Mahmood), aflehlooh@yu.edu.jo (A.-F. Lehlooh).
[1] Tel.: +962 2 721 1111x2071; fax: +962 2 721 1121.
[2] Tel.: +962 2 721 1111x2328; fax: +962 2 721 1117.

0925-8388/$ – see front matter © 2010 Elsevier B.V. All rights reserved.
doi:10.1016/j.jallcom.2010.03.142

Table 1
Values of the anisotropy constant K_1 associated with a single Fe^{3+} ion at the different sites in barium hexaferrite (Ref. [33]).

Site	$4f_1$	$4f_2$	$2a$	$12k$	$2b$
K_1 (cm^{-1}/ion)	0.18	0.51	0.23	−0.18	1.40

the largest positive contribution to the anisotropy field at the $2b$ site, a relative weak positive contribution at the $4f_1$, $4f_2$, and $2a$ sites, and a negative contribution at the $12k$ site as illustrated in Table 1. Hence the substitution of Fe^{3+} ions at different lattice sites leads to different contributions to the magnetic anisotropy field.

The present work is concerned with the effect of Ti–Ru substitution for Fe on the magnetic properties of barium hexaferrites synthesized by ball milling method. Vibrating sample magnetometry, X-ray diffraction (XRD), Mössbauer spectroscopy and electron microscopy have been employed to characterize the fabricated powders and investigate their magnetic behavior.

2. Experimental procedures

$BaFe_{12-2x}Ti_xRu_xO_{19}$ powders with $x = 0.0$, 0.1, 0.2, 0.3 and 0.4 were prepared by ball milling method. High purity metallic oxides (Fe_2O_3, TiO and RuO_2) and barium carbonate ($BaCO_3$) were used as starting materials. The ratio of iron to barium was set at Fe/Ba = 11, which is according to our experience, the optimum ratio that gives single phase diffraction pattern. Mechanical alloying was performed in a planetary ball-mill (Fritsch Pulverisette 7) using a ball to powder ratio of 8:1. Milling was carried out for 16 h with an angular frequency of 250 rpm. After mechanical milling, the mixture was pressed into disks, 1 cm in diameter under a force of 50 kN. These disks were annealed in air atmosphere at 1100 °C for 2 h.

XRD analysis was carried out using Philips X'Pert PRO X-ray diffractometer (PW3040/60) with Cu K_α radiation. The magnetic measurements were carried out using a vibrating sample magnetometer (VSM MicroMag 3900, Princeton Measurements Corporation), with a maximum applied field of 10 kOe. The isothermal remanent magnetization (IRM) curve was obtained by the following procedure: the sample was initially demagnetized. A small positive field was applied then removed, and the remanence magnetization was recorded. The procedure was repeated with increasing the positive field until the saturation remanence was reached.

3. Results and discussion

XRD patterns of $BaFe_{12-2x}Ti_xRu_xO_{19}$ samples, along with the standard pattern for hexagonal barium ferrite ($BaFe_{12}O_{19}$) with space group $P6_3/mmc$ (JCPDS file no: 043-0002) [34] are shown in Fig. 1. It can be seen that the XRD patterns for all samples match the standard pattern for hexagonal barium ferrite ($BaFe_{12}O_{19}$), with less than 0.2% change in lattice parameters, and with similar relative intensity profiles for all observed peaks. No secondary phases were detected, within the detection limit of the technique for all doping values inspected in this work. The small increase of c (0.17%) might be a result of ionic size effect, since the radius of Fe^{3+} ion (0.645 Å) is smaller than that for Ti^{2+} (1.0 Å) and for Ru^{4+} (0.67 Å).

The average crystallite size was determined from the positions of the (2 1 7) and (2 2 0) reflections using the well-known Scherrer formula [35],

$$D = \frac{k\lambda}{\beta \cos\theta}, \quad (3)$$

where D is the crystallite size, k the Scherrer constant, λ the wavelength of radiation (1.54056 Å), β the peak width at half maximum measured in radians, and θ the peak position. The average crystallite size for the pure sample is found to be 42 nm, while that for the doped samples is found to be in the range from 69 (for $x = 0.1$) to 77 nm (for $x = 0.4$), which indicates that the crystallinity of the samples improves with the substitution.

TEM imaging (Fig. 2) shows that the average grain size of all substituted hexaferrites is similar, and they possess a broad particle size distribution. The average particle size increases from (42 ± 13) nm for the pure sample up to (180 ± 45) nm with substitution. These particle sizes are smaller than the critical value of

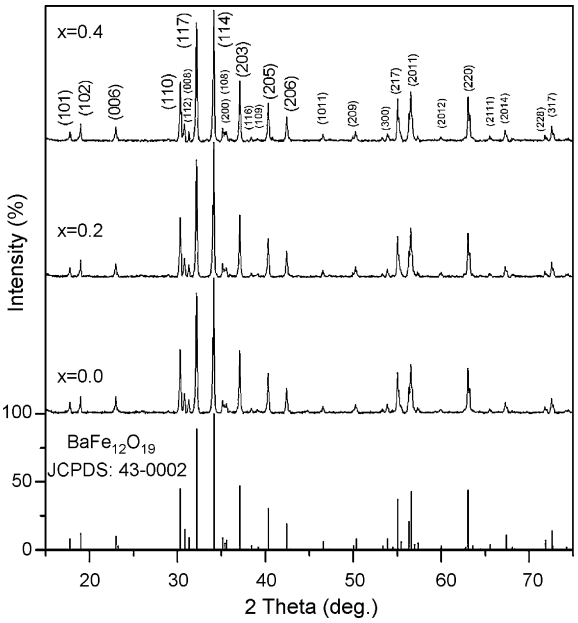

Fig. 1. Standard JCPDS pattern for M-type hexagonal barium ferrite (file no: 043-0002) and XRD patterns of $BaFe_{12-2x}Ti_xRu_xO_{19}$ with different doping concentrations.

460 nm reported by Rezlescu et al. [36] for a single magnetic domain particle, which indicates that all samples consist of single magnetic domain particles.

Mössbauer spectra at room temperature for representative samples are shown in Fig. 3. The spectra were fitted with four magnetic sextets corresponding to the five crystallographic sites of the Fe ions, since the components corresponding to the $2a$ and $4f_1$ sites could not be resolved due to their similar hyperfine parameters [37]. Due to the small substitution levels, the areas of the subspectra could not reveal accurate information on the preferential site occupation of the Ru^{4+} and Ti^{2+} ions (variations in the areas are ~1–2% which is within experimental uncertainty). Thus the hyperfine interactions are used to deduce such information. The hyperfine field and quadrupole splitting vs. x are shown in Fig. 4. Fig. 4a shows that the hyperfine fields corresponding to the $4f_2$ and $2a + 4f_1$ sites decrease almost linearly with x, while that corresponding to the $2b$ site is almost constant up to $x = 0.1$, and then decreases slightly with increasing x. On the other hand, the hyperfine field corresponding to the $12k$ site remains almost constant. Fig. 4b shows that the quadrupole splittings corresponding to the $4f_2$ and $2a + 4f_1$ sites vary up to $x = 0.2$, and then remain constant for higher substitutions. On the other hand the quadrupole splitting for the $2b$ site changes appreciably for $x > 0.1$. Further, the hyperfine parameters corresponding to the $12k$ site are almost unaffected by the substitution. The variations of the hyperfine interactions indicate that as x increases up to 0.2, the substitution for Fe occurs mostly at the $4f_2$ and $2a + 4f_1$ sites, and for $x \geq 0.2$, the $2b$ site starts to be substituted. However, the $12k$ site is not affected by the substitution over the whole range of x. Since ions with larger radii tend to occupy octahedral sites, and those with smaller radii tend to occupy tetrahedral and bipyramidal sites, we conclude that Ti^{2+} occupy the $4f_2$ and $2a$ sites, while Ru^{4+} occupy the $4f_1$ and $2b$ sites, which is consistent with previous studies on Ni–Ru and Zn–Ru substituted hexaferrites [37].

Hysteresis loops for the samples were measured as a function of applied magnetic field and the results are shown in Table 2. The magnetization for the pure sample is characteristic of a hard magnetic material with coercive field strength of 4 kOe. This value of the coercivity agrees well with previous reports on samples prepared by sol–gel method [30] and mechanical alloying method

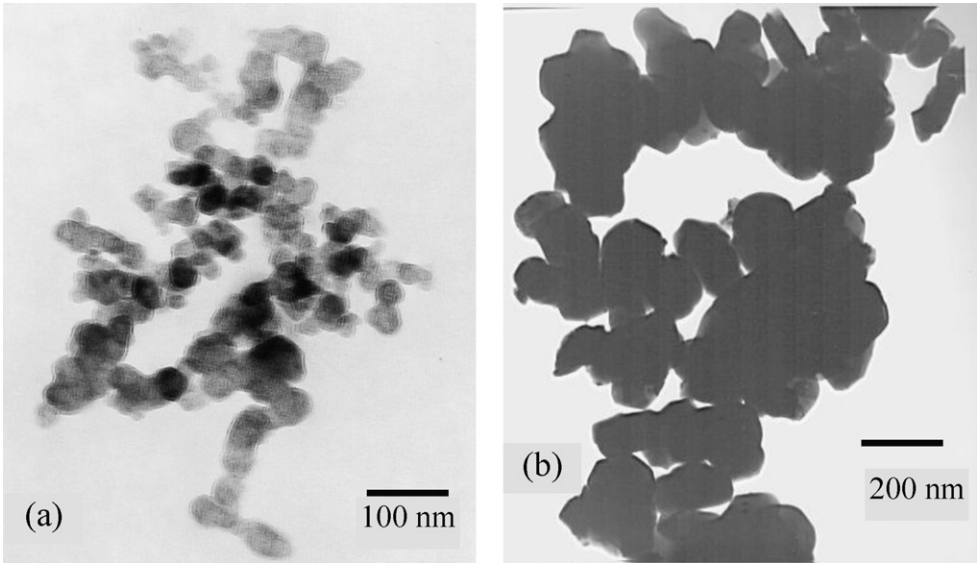

Fig. 2. TEM images of $BaFe_{12-2x}Ti_xRu_xO_{19}$, (a) $x = 0.0$ and (b) $x = 0.4$.

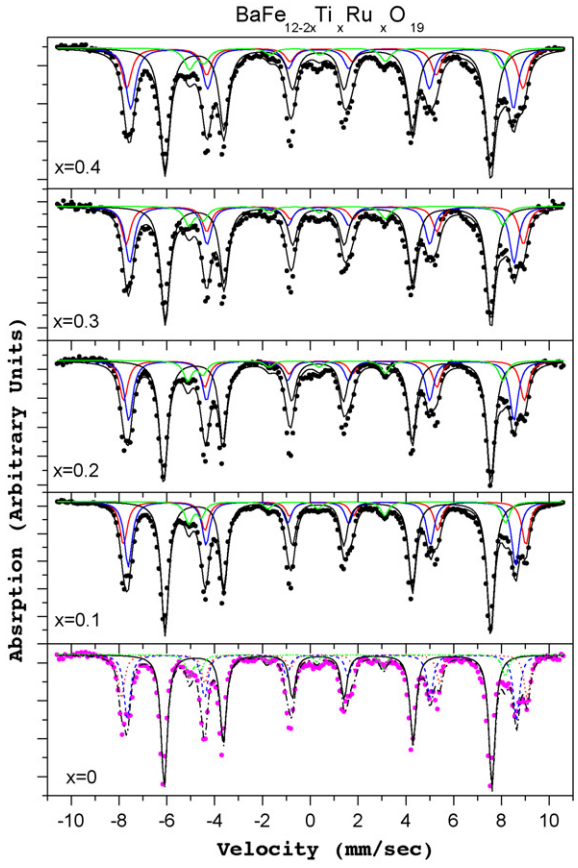

Fig. 3. Room temperature Mössbauer spectra for $BaFe_{12-2x}Ti_xRu_xO_{19}$ samples.

Table 2
Coercivity, saturation magnetization, and Curie temperature of $BaFe_{12-2x}Ti_xRu_xO_{19}$.

x	H_c (kOe)	M_s (emu/g)	T_c (°C)
0.0	4.0	59.7	505
0.1	3.3	65.3	482
0.2	2.4	68.3	482
0.3	2.1	66.7	481
0.4	1.8	64.3	481

[28,38]. The effect of Ti–Ru content on the saturation magnetization and coercivity of $BaFe_{12-2x}Ti_xRu_xO_{19}$ for all samples examined is shown in Fig. 5. The saturation magnetization initially increases for x between 0.0 and 0.2 (increase in M_s is 11%), and then decreases for x between 0.2 and 0.4, recording a reduction of ~8% at $x = 0.4$. Based on the simple model in Eq. (1), the increase in the saturation magnetization is attributed to the replacement of $4f_1$ and $4f_2$ spin-down Fe^{3+} ions by paramagnetic Ru^{4+} and Ti^{2+} ions, respectively. The observed drop in the saturation magnetization in the concentration range $x = 0.2$–0.4 is associated with the replacement of Fe^{3+} ions by Ti^{2+} and Ru^{4+} ions at the $2a$ and $2b$ spin-up sites, respectively. These results are consistent with the Mössbauer data above, and agree well with those reported by Gonzalez-Angeles et al. [37] who have observed ~9% increase in M_s upon substituting Fe by Zn–Ru ($x = 0.3$) and ~7% increase upon substituting by Ni–Ru.

Fig. 5 also shows that with increasing Ti–Ru doping, the value of the coercivity decreases monotonically for all samples examined, recording a drop of 55% at $x = 0.4$. Such a drop in the coercivity, along with a small decrease in saturation magnetization, was observed by others [13,18]. Thus, a small substitution of Fe by Ti–Ru results in a substantial reduction in the coercivity, and improvement in the saturation magnetization, which are favorable for high density magnetic recording applications.

The sharp decrease of the coercivity in the range $x \leq 0.2$ is associated with the sharp decrease in anisotropy field (H_a) as a result of the combined effect of the replacement of Fe ions at the $4f_1$ and $4f_2$ sites, and the sharp increase in saturation magnetization as can be deduced from Eq. (2). For $x > 0.2$, the negative slope of the coercive field decreases in spite of the onset of partial substitution of Fe^{3+} ions at the $2b$ site which contributes highly to the magnetic anisotropy. This is a consequence of the competing effects of the reduction of H_a due to substitution, and the increase due to the drop in M_s in this range of x.

In order to investigate the correlation between the coercivity and the magnetic anisotropy field in our system, we determine the effective magnetic anisotropy field for each sample examined in this work from the switching field distribution (SFD). The switching field distribution can be obtained by differentiating the reduced IRM curve $m_r(H) = M_r(H)/M_r(\infty)$. Fig. 6 shows the reduced IRM curve and the corresponding switching field distribution for the samples with $x = 0.0$ and 0.3. The effective magnetic anisotropy field for each sample examined in this work is obtained from the maximum of

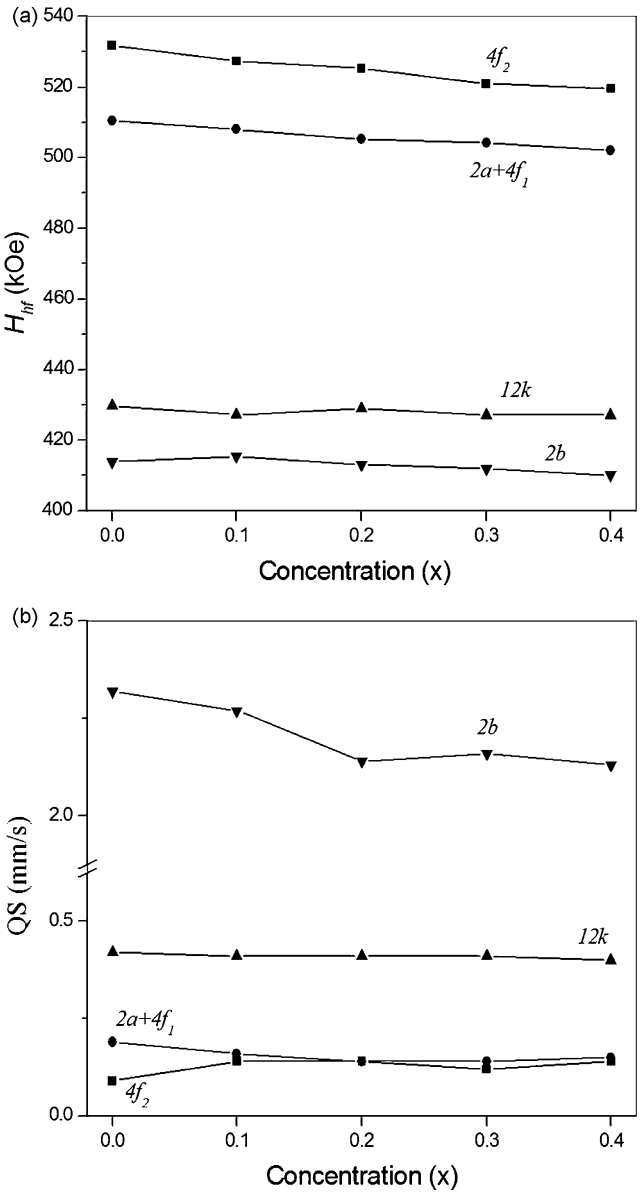

Fig. 4. (a) Hyperfine field (H_f) and (b) quadrupole splitting (QS) for the different sites in $BaFe_{12-2x}Ti_xRu_xO_{19}$ as a function of Ti–Ru concentration (x).

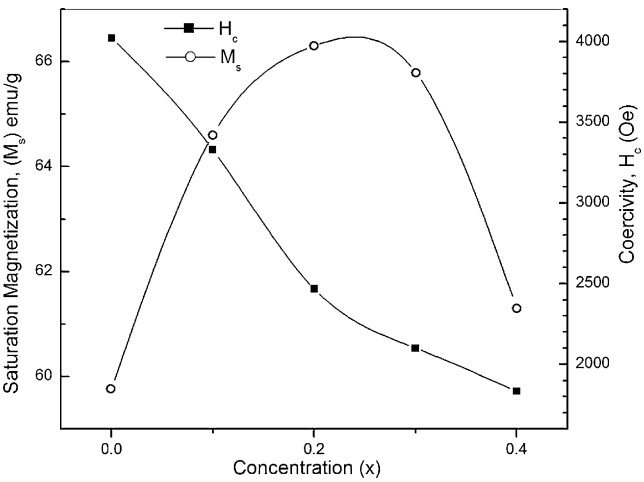

Fig. 5. Saturation magnetization and coercivity of $BaFe_{12-2x}Ti_xRu_xO_{19}$ as a function of Ti–Ru concentration (x).

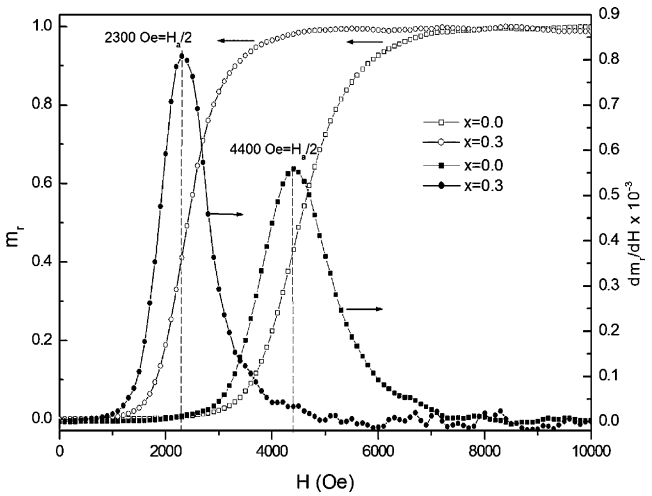

Fig. 6. Reduced IRM curves and switching field distributions for the samples with $x = 0.0$ and $x = 0.3$.

the switching field distribution [39]:

$$f(H)]_{\max} = \left[\frac{dm_r}{dH}\right]_{H=H_a/2} \quad (4)$$

Here $H_a = 2H_{\max}$, where $H_{\max}$ is the value of the field at the maximum of the SFD. Fig. 7 shows the variation of magnetic anisotropy field with Ti–Ru concentration for all samples examined. It is clear that H_a decreases rather sharply with increasing Ti–Ru concentration up to $x = 0.2$, and then starts leveling off for higher concentrations as discussed earlier. The ratio H_c/H_a for all sample is in the range 0.4–0.46, which is close to the ratio of 0.48 expected from the Stoner–Wohlfarth model for single-domain, non-interacting, randomly oriented particles [40]. The small deviation from the model value could be associated with the geometry of the particles in our system, and partially with small particle–particle interactions.

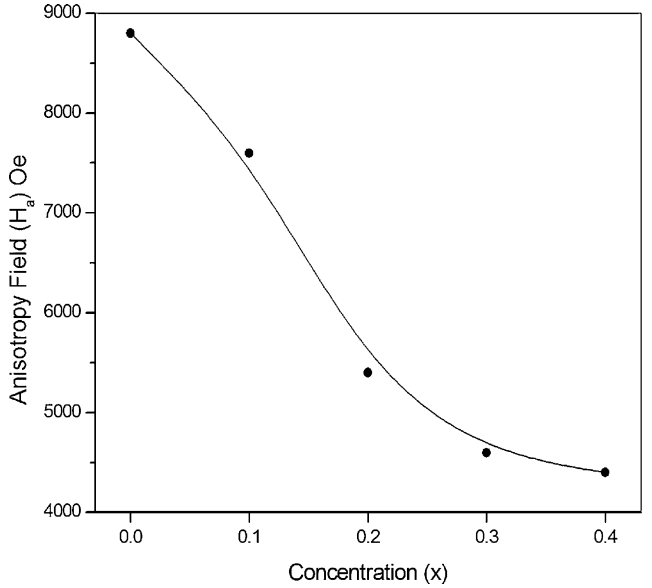

Fig. 7. Anisotropy field of $BaFe_{12-2x}Ti_xRu_xO_{19}$ as a function of the Ti–Ru concentration (x).

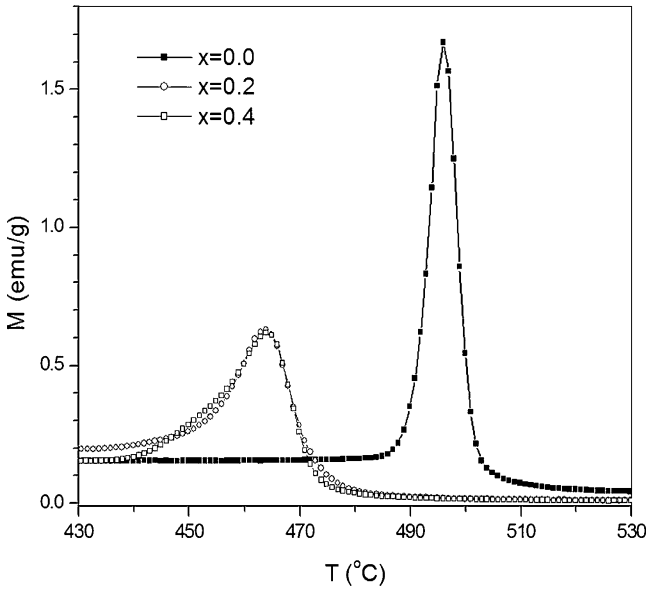

Fig. 8. Magnetization as a function of temperature for $BaFe_{12-2x}Ti_xRu_xO_{19}$ with $x = 0.0$, 0.2, and 0.4 at a constant applied field of 100 Oe.

Fig. 8 shows the magnetization as a function of temperature $M(T)$ around T_c for the samples with $x = 0.0$, 0.2 and 0.4 at a small applied field of 100 Oe. From these curves one might obtain T_c, which is defined as the temperature at the bottom of Hopkinson peak. Curie temperature as a function of Ti–Ru concentration in $BaFe_{12-2x}Ti_xRu_xO_{19}$ is shown in Table 2. It is found that Curie temperature is constant for all substitutions, which is about 5% lower than that for the pure sample (~505 °C). This is consistent with the drop in T_c observed in the Zn–Ru and Ni–Ru substituted systems [37]. The sharpness of the Hopkinson peak for the pure sample indicates a narrow size distribution, yet the peaks for all substituted samples are similarly broad, indicating a broad particle size distribution as confirmed by the TEM measurements. The value of $M(T)$ at the peak for the pure sample is 10.8 times larger than that at the minimum, which is consistent with the calculated value for a system of non-interacting, randomly oriented, uniaxial single-domain particles [41]. This indicates that the particle size of (42 ± 13) nm for this sample measured by TEM is in the superparamagnetic (SP) regime. Further, the value of $M(T)$ at the peak drops substantially to 3.2–4 times the minimum value for all substituted samples. This drop is associated with the significant increase in particle size for the substituted samples, which leaves only a small fraction of the particles in the superparamagnetic regime responsible for the relatively weak peak. Following the theoretical calculation of the magnetization in [41], the mass fraction f of the SP particles in the substituted samples can then be evaluated from the relation:

$$M_p = fM_{SP} + (1 - f)M_m \quad (5)$$

where M_p is the magnetization at the peak, M_{SP} the magnetization due to the SP particles, and M_m the minimum magnetization due to the remaining (blocked) particles. Assuming that the pure sample consists of SP particles only we obtain the relation: $M_{SP} = 10.8\,M_m$. Using Eq. (5) with our experimental peak values of 3.2–4.0 times higher than the minimum value for the substituted samples, we conclude that the fraction of SP particles in these samples is only 22–30%.

4. Conclusions

The substitution of Fe^{3+} ions by Ti^{2+} and Ru^{4+} ions in $BaFe_{12-2x}Ti_xRu_xO_{19}$ resulted in an increase in particle size, a broadening of the particle size distribution, and an improvement of the sample crystallinity. The substitution was found to occur at the $4f_2$ and $4f_1$ sites for x values up to 0.2, resulting in a sharp initial increase in M_s and a consequent sharp reduction in coercivity. Substitution at the $2a$ and $2b$ sites was found to occur for $x \geq 0.2$ as well, resulting in the observed maximum in M_s at about $x = 0.2$, and the consequent reduction in the negative slope of the coercivity above this concentration. Hopkinson peak was observed in the thermomagnetic curves for all samples, and indicated that the pure sample is purely superparamagnetic, while the substituted samples are only 22–30% superparamagnetic.

References

[1] F. Kools, A. Morel, R. Grossinger, J.M. Le Breton, P. Tenaud, J. Magn. Magn. Mater. 242–245 (2002) 1270.
[2] T. Fujiwara, IEEE Trans. Magn. 21 (1985) 1480.
[3] Y.J. Chen, M.H. Kryder, J. Appl. Phys. 78 (8) (1996) 4878.
[4] D.E. Speliotis, IEEE Trans. Magn. 31 (1995) 2877.
[5] J. Kreisel, H. Vincent, F. Tasset, P. Wolfers, J. Magn. Magn. Mater. 213 (2000) 262.
[6] H. Pfeiffer, R.W. Chantrell, P. Gornert, W. Schuppel, E. Sinn, M. Rosler, J. Magn. Magn. Mater. 125 (1993) 373.
[7] G. Li, G. Hu, H. Zhou, X. Fan, X. Li, Mater. Chem. Phys. 75 (2002) 101.
[8] N. Dishovske, A. Petkov, IEEE Trans. Magn. 30 (1994) 969.
[9] A. Ghasemi, A. Morisako, J. Alloys Compd. 456 (2008) 485.
[10] X. Tang, Y. Yang, K. Hu, J. Alloys Compd. 477 (2009) 322.
[11] G. Litsardakis, I. Manolakis, K. Efthimiadis, J. Alloys Compd. 427 (2007) 194.
[12] D. Ravinder, P. Shalini, P. Mahesh, K.K. Rao, M. Vithal, B.S. Boyanov, J. Alloys Compd. 364 (2004) 17.
[13] G.B. Teh, N. Saravanan, D.A. Jefferson, Mater. Chem. Phys. 105 (2007) 253.
[14] F. Tabatabaie, M.H. Fathi, A. Saatchi, A. Ghasemi, J. Alloys Compd. 474 (2009) 206.
[15] Ch. Venkateshwarlu, Ch. Ashok, B.A. Rao, D. Ravinder, B.S. Boyanov, J. Alloys Compd. 426 (2006) 1.
[16] M.J. Iqbal, M.N. Ashiq, P.H. Gomez, J. Alloys Compd. 478 (2009) 736.
[17] F. Tabatabaie, M.H. Fathi, A. Saatchi, A. Ghasemi, J. Alloys Compd. 470 (2009) 332.
[18] Y. Li, R. Liu, Z. Zhang, C. Xiong, Mater. Chem. Phys. 64 (2000) 256.
[19] J. Qiu, L. Lan, H. Zhang, M. Gu, J. Alloys Compd. 453 (2008) 261.
[20] M. Han, Y. Ou, W. Chen, L. Deng, J. Alloys Compd. 474 (2009) 185.
[21] A. Ataie, S.E. Zojaji, J. Alloys Compd. 431 (2007) 331.
[22] T. Yamauchi, Y. Tsukahara, T. Sakata, H. Mori, T. Chikata, S. Katoh, Y. Wada, J. Magn. Magn. Mater. 321 (2009) 8.
[23] U. Topal, H. Ozkan, L. Dorosinskii, J. Alloys Compd. 428 (2007) 17.
[24] P. Xu, X. Han, H. Zhao, Z. Liang, J. Wang, Mater. Lett. 62 (2008) 1305.
[25] S. Chaudhury, S.K. Rakshit, S.C. Parida, Z. Singh, K.D. Singh Mudher, V. Venugopal, J. Alloys Compd. 455 (2008) 25.
[26] K.S. Moghaddam, A. Ataie, J. Alloys Compd. 426 (2006) 415.
[27] G. Mendoza-Suarez, J.A. Matutes-Aquino, J.I. Escalante-Garcia, H. Mancha-Molinar, D. Rios-Jara, K.K. Johal, J. Magn. Magn. Mater. 223 (2001) 55.
[28] V. Babu, P. Padaikathan, J. Magn. Magn. Mater. 241 (2002) 85.
[29] S. Wang, J. Ding, Y. Shi, Y.J. Chen, J. Magn. Magn. Mater. 219 (2000) 206.
[30] S.Y. An, I.B. Shim, C.S. Kim, J. Appl. Phys. 91 (10) (2002) 8465.
[31] X.Z. Zhou, A.H. Morrish, Z.W. Li, Y.K. Hong, IEEE Trans. Magn. 27 (6) (1991).
[32] J.M. Williams, J. Adetunji, M. Gregori, J. Magn. Magn. Mater. 220 (2000) 124.
[33] Y. Xu, G.L. Yang, A.P. Chu, H.R. Zhai, Phys. Status Solidi (B) 157 (1990) 685.
[34] International Centre for Diffraction Data (ICDD), JCPDS File 43-0002.
[35] B.E. Warren, X-ray Diffraction, Addison-Wesley, Reading, MA, 1969.
[36] L. Rezlescu, E. Reslescu, P.D. Popa, J. Magn. Magn. Mater. 193 (1999) 288.
[37] A. Gonzalez-Angeles, G. Mendoza-Suarez, A. Gruskova, J. Lipka, M. Papanova, J. Slama, J. Magn. Magn. Mater. 285 (2005) 450.
[38] P. Sharma, R.A. Rocha, S.N. de Medeiros, A. Paesano Jr., J. Alloys Compd. 443 (2007) 37.
[39] H. Pfeiffer, W. Schüppel, Phys. Status Solidi (a) 119 (1990) 259.
[40] P. Görnert, W. Schüppel, E. Sinn, F. Schumacher, K.A. Hempel, G. Turilli, A. Paoluzi, M. Rösler, J. Magn. Magn. Mater. 114 (1992) 193.
[41] H. Pfeiffer, W. Schüppel, J. Magn. Magn. Mater. 130 (1994) 92.